

Study of Mechanical, Thermal, and Microstructural Properties of Polypropylene/Ceramic Waste Composites

Roberto LÓPEZ-RAMIREZ¹, Ana L. FLORES-VAZQUEZ²,
Victor CASTREJON-SANCHEZ¹, Lucía TELLEZ-JURADO³,
Hector J. DORANTES-ROSALES³, Orlando SORIANO-VARGAS^{1*}

¹ Tecnológico de Estudios Superiores de Jocotitlán, Jocotitlán, C.P. 50700, México

² Universidad Autónoma del Estado de México, C.P. 52640, México

³ Instituto Politécnico Nacional, Ciudad de México, C.P. 07738, México

<https://doi.org/10.5755/j02.ms.30947>

Received 23 March 2022; accepted 26 October 2022

In this work, the effect of reinforcement of the iPP with ceramic waste (CW), and the use of maleic anhydride compatibilizing agent grafted with polyolefin elastomer (POE-g-MAH) are studied. The composites were fabricated by extrusion and injection processes, and their morphology and microstructure, as well as fracture surface and mechanical and thermal properties, were analyzed. Characterization by polarized optical microscopy showed that the ceramic waste particles were well-dispersed into the iPP matrix without the presence of agglomerates. However, the POE-g-MAH did not show good compatibility when it was added to the iPP/CW composite. Hardness Rockwell R, tensile and flexural measurements showed that the hardness, Young's modulus, and flexural modulus increased with the incorporation of CW and without the POE-g-MAH. The ductility of the composites was several decreased with the addition of CW. POE-g-MAH affected the hardness, ductility, strength tensile, Young's modulus, flexural modulus, and interfacial interaction in the iPP/CW composite. Analysis by X-ray diffraction showed that the CW also acted as a nucleating agent, increasing the crystallization degree, and forming the β -phase. Analysis of the Fourier-transformed infrared showed transmittance bands of the iPP, CW, POE-g-MAH and composites. The bands were similar and there were no major changes in characteristic bands of composites, but CW, and POE-g-MAH produced changes in the shape and intensity of band peaks of the iPP matrix. The CW addition to the iPP matrix modified the thermal properties of pure iPP, such as the degree of crystallization and melting temperature in the iPP/CW composites. The incorporation of POE-g-MAH decreased the crystallization temperature and crystallinity degree in the iPP/CW composite.

Keywords: ceramic waste, isotactic polypropylene, mechanical properties, thermal properties, POE-g-MAH.

1. INTRODUCTION

The foundry industry produces a lot of by-products or solid wastes such as fly ash, bottom ash, waste foundry sand, slag, silica fume, shell waste, asbestos, and glass waste. Those industrial wastes [1–3], and environmental pollution are some of the factors responsible for searching for new solutions for sustainable development. This sustainability can only be achieved if efficiency in the use of natural resources and waste increases [4]. The foundry sand waste, especially for this work has been focused on using the waste that one generated in the investment casting process. Refractory waste is an interesting candidate to be used as a sustainable material inside of circular economy, therefore, large amounts of refractory dust are produced daily (~1 ton/day, data of manufacturing company and [5]) because of the demolding of the solidified metal, and in most cases, refractories are disposed for the landfill wasting valuable natural resources. These kinds of wastes contain compounds such as firstly mullite, zircon, and others such as silica, alumina, and iron oxides, among others. Those are part of the shell mold that support high temperature about 1600 °C, and consequence strength mechanical, and resistance in high temperature. And then, they can be used

as fillers in polymers matrix composite. Currently, it had been the development of polymer matrix composites reinforced with inorganic particles for the improvement of the mechanical properties and thermal properties [6]. Thus, ceramic waste (CW) based on mullite ($3Al_2O_3-4SiO_2$) becoming increasingly important in electronic, optical, and high temperature structural applications, because of its low dielectric constant, good transparency for mid-infrared light, excellent creep resistance, low thermal expansion, low thermal conductivity, and good chemical stability [7]. The zircon has similar properties, such as excellent creep resistance, low thermal expansion, low thermal conductivity, and good chemical stability [6]. CW should be used in some polymer matrices to reinforce them. The application of this type of reinforcement could be for structural components.

Polypropylene (PP) is a semicrystalline polymer used in polymer matrix composite due to its excellent mechanical, chemical, and thermal properties as well as its low density and easy processing with heat distortion temperature above 100 °C, and low cost. Also, due to the large amount of waste generated from this highly consumed plastic worldwide [8].

* Corresponding author. Tel.: +7222898770.

E-mail: orlando.soriano@tesjo.edu.mx (O. Soriano-Vargas)

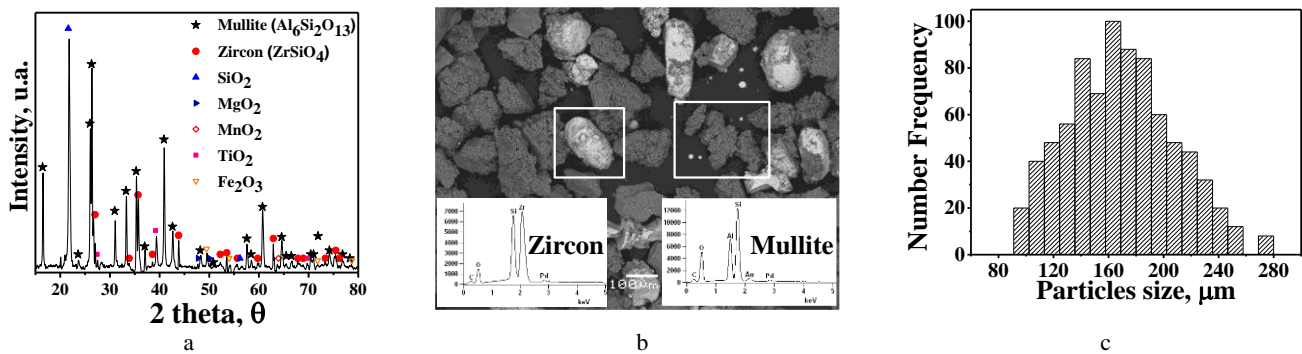


Fig. 1. a – XRD pattern of ceramic waste; b – SEM morphology and EDS elemental analysis of CW; c – particle sizes distribution of CW

However, the poor flexure and impact resistance of PP limits its application in some devices. It is common that the PP is to be mixed with other polymers or filled with inorganic particles for reinforcement of the impact resistance or other properties. Some fillers used are CaCO_3 , Al_2O_3 , glass, mica, SiO_2 , montmorillonite, and wollastonite [8–10]. Nevertheless, the homogeneous dispersion of fillers due to the hydrophobic nature of the polymer molecules difficult the use of inorganic particles in the PP matrix, which is solved by the addition of compatibilizing agents such as maleic anhydride grafted, among others [11], is required to improve the adhesion between the matrix and fillers.

Poly(ethylene-co-octene) (POE) is a polyolefin elastomer with narrow molecular weight distribution and homogenous octene distribution, and it is often blended with other compounds such as maleic anhydride (MAH) for compatibilization purposes [12]. Zhong *et al.* [13] reported the addition of different amounts (from 0 to 20 wt.%) of POE-g-MAH compatibilizer in PP-clay blends has improved the compatibility and mechanical properties of blends raising the degree of compatibilization between iPP matrix with clay. Also, studies of PP matrix composites with nanofillers using POE-g-MAH as a compatibilizing agent show greatly increased impact strength values [14–16]. Qiao *et al.* [17] studied the thermal properties in PP/POE-g-MAH/clay (PPMC) nanocomposites with different amounts of nano-clay. The study suggests that the nucleation role of POE-g-MAH on PP crystallization is gradually decreased as the clay content increases from 3 to 7 wt.%. Also, the blending of POE-g-MAH into the iPP matrix raises the thermal enthalpy of PP, especially the melting enthalpy, while the addition of clay further strengthens this effect. Lin *et al.* [18] mentioned that POE-g-MAH facilitates the dispersion of recycled corrugated paper with a particle size of less than 100 μm in the iPP matrix.

Therefore, the application of iPP and the ceramic waste particles of mullite and zircon, and POE-g-MAH has not been reported, which will allow understanding of their interaction and as a result, the mechanical and thermal properties to determine their potential structural application, and promote the sustainability of ceramic waste. The purpose of this work is to study virgin isotactic polypropylene (iPP) matrix and the effect of the ceramic waste (CW) and polyolefin elastomer grafted maleic anhydride (POE-g-MAH) in the microstructure, mechanical properties, and thermal properties.

2. EXPERIMENTAL

2.1. Materials

Isotactic polypropylene (iPP) homopolymer (Indelpro Valtec Company (HS013)) with melt flow rate (MFR) of 9.0 g/10 min at 230 $^{\circ}\text{C}$, density $\rho = 0.9 \text{ g/cm}^3$ and weight molecular $M_n = 120,000 \text{ g/mol}$. Yield strength 33 MPa, flexure modulus 1.484 GPa, hardness Rockwell R 98.

The ceramic waste (CW) was obtained from a manufacturing investment casting process. The compounds in the CW were verified by DRX Bruker AXS (Advanced X-Ray solutions) D8 X-ray diffractometer with a $\text{Cu K}\alpha$ ($\lambda = 1.5406 \text{ \AA}$) radiation (Fig. 1 a), and the corresponding number pattern: mullite- $\text{Al}_6\text{Si}_2\text{O}_{13}$ (0-015-0776), zircon- ZrSiO_4 (780-790), SiO_2 (00-027-0605), Fe_2O_3 (82-0598), MgO 00-019-0771, TiO_2 (00-034-01807), MnO_2 (00-043-1455).

Polyolefin elastomer grafted maleic anhydride (POE-g-MAH) (Dow-Amplify Company) with a melt index of 1.3 g/10 min, tensile strength 8.96 MPa, flexural modulus 13.8 MPa, the density of 0.875 g/cm^3 was used for compatibilization of the iPP matrix with the CW particles.

2.2. Composite processing

2.2.1. Preparation CW

The CW particles were obtained using a 200 μm mesh. Fig. 1 b shows by scanning electron microscopy (SEM-EDS, JEOL 100 microscope with an accelerating voltage of 15 kV, WD 15 mm, secondary electron), images of the CW particles showed mullite (grey particles) with an irregular morphology and zircon particles (white particles) with rounded morphology are observed. The EDS analysis confirms the elements corresponding to each particle. The mean particle size of CW was measured, and their mean particle size was about 169 μm , see Fig. 1 c. The CW was dried in a drying oven at 105 $^{\circ}\text{C}$ for 24 h prior to blending them with the iPP. Similarly, the iPP pellets and the POE-g-MAH were dried at 80 $^{\circ}\text{C}$ for 20 h.

2.2.2. Preparation of composites

The extrusion process was carried out using an extrusion machine (Beutelspacher) with a twin-screw. The temperatures from the feeder zone to the extrusion die zone were maintained at 200, 250, 235, 230, and 200 $^{\circ}\text{C}$. Injection molding temperatures were set between 195, 200, 210, and 220 $^{\circ}\text{C}$ in the barrel, and the cooling time was 35 s inside the mold. The screw speed was 150 rpm, and the

injection pressure was maintained at 65 MPa. Finally, the tensile and flexural test samples were obtained to determine the mechanical properties. Table 1 shows the composition weight percent (wt.%) of pure iPP and composites, and the computed density of composite samples.

2.3. Instruments and methodology

The morphology, fracture surface, and particle size of CW in the iPP matrix of the composite were examined using scanning electron microscopy (SEM) using a JEOL IT100 microscope with an accelerating voltage of 15 kV. Samples were taken from the tensile and flexural fracture surfaces of composites and pure iPP before the analysis. Additionally, the CW particle dispersion was examined with a polarized light optical microscopy (OM) VELAB 407.

Table 1. Composition and density computer data of pure iPP and composites

Sample	iPP, wt.%	Ceramic waste, wt.%	POE-g-MA, wt.%	Density, g/cm ³
CW	–	–	–	3.3
iPP	100	0	0	0.920*
POE-g-MAH	–	–	–	0.875*
Ci50	95	5	0	0.998
Ci53	92	5	3	1.043
Ci55	90	5	5	1.042
Ci100	90	10	0	1.170
Ci103	87	10	3	1.167
Ci105	85	10	5	1.146

* Specification company

The mechanical properties were carried out using an Instron 3365 universal testing machine (5 kN capacity). The iPP/CW composite probe samples used for tensile and flexural tests were fabricated according to the standard ASTM D638 and ASTM D790, respectively. The elasticity modulus, the strength tensile, and the elongation at break (ductility) values were determined for the tensile test. The sample bend testing was cooled with nitrogen at -30 °C. Flexural stress and flexure modulus values were also determined. The maximum percentage strain applied to all iPP/CW composite probe samples was 30 %. For each iPP and composites samples of each mechanical test, 10 specimens were tested, see Table 1.

The hardness Rockwell R (HRR) tests were carried out in a Rockwell Digital DRS150 equipment with a ball diameter of 12.7 mm, according to the standard ASTM D785. The pre-load applied to the iPP/CW composite samples was 98.07 N (10 kg), and the load was 588.9 N (60 Kg). The dwell time was 10 s. The tests were performed at room- temperature and 5 indentations were made for each of the sample conditions, see Table 1. X-Ray Diffraction analysis (XRD) was conducted in a Bruker AXS (Advanced X-Ray solutions) D8 X-ray diffractometer with a Cu K α (λ -1.5406 Å) radiation. The crystallite size of the composite was calculated using Scherrer's equation [19]:

$$L_{hkl} = \frac{K \lambda}{\beta \cos \theta}, \quad (1)$$

where λ is the wavelength, $K = 0.94$; β is the full-width half maxima perpendicular to each plane; θ is the Bragg's angle.

Fourier Transform-Infrared Spectroscopy (FTIR) analysis was performed in the transmission mode with a Nicolet-560 spectrometer. The spectra were collected at 2 cm⁻¹ resolutions between 400 and 4000 cm⁻¹ with collection times of approximately 1 min.

Differential scanning calorimetry (DSC) and Thermogravimetric analysis (TGA) techniques were used to analyze the thermal behavior, loss of weight, and thermal transition of the iPP and the iPP/CW composite. The thermal analyses were done in a simultaneous DSC-TGA Q20 V 24.4 Build 116 (TA Instruments, New Castle, DE, USA), with a heating rate of 10 °C/min from 50 to 400 °C in a nitrogen atmosphere. The weight of the samples was in the range of 5 – 15 mg.

3. RESULTS AND DISCUSSION

3.1. Dispersion CW studies by OM

Fig. 2 a and b show a comparison of OM micrographs of the Ci55 and Ci10 (5 and 10 wt.%). The composites showed a homogeneous mixture and well-dispersion of the CW particles into the iPP matrix without the presence of agglomerates. The presence of POE-g-MAH compatibilizer did not affect the particle well-dispersion of the CW in the polymer matrix, see Fig. 2 c and d [17].

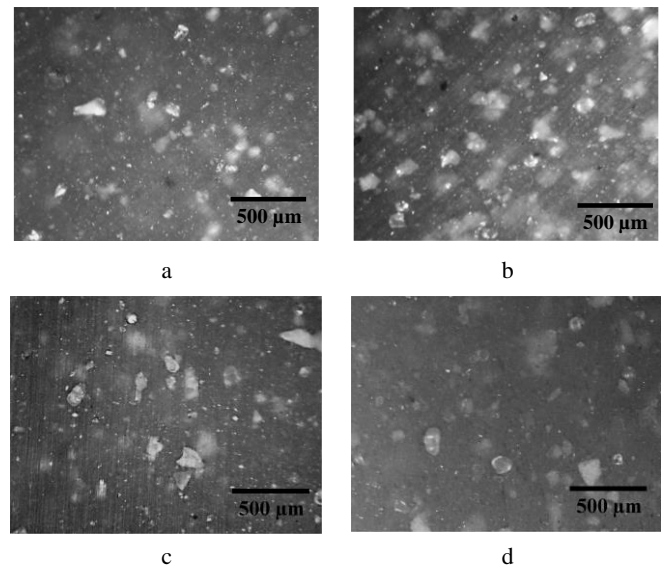


Fig. 2. OM images of composite: a–Ci50; b–Ci100; c–Ci55; d–Ci105 with 5 wt.% of POE-gMAH, both

3.2. Mechanical properties of composites

The mechanical properties of pure iPP, iPP/CW, and iPP/CW/POE-g-MAH composites were shown in Fig. 3, Fig. 4, and Fig. 5. First observation, the tensile test was the ductility. The pure iPP and composites were evaluated using the stress-strain curve shown in Fig. 3 a. The pure iPP exhibits ductility until 500 % of strain at room temperature. Ci50 and Ci100 composites show a drastic reduction of the ductility until 31 and 29 %, this is due to the addition of the CW to the iPP, which indicates that the CW particles restricted the flow of polymer molecules past one another and caused a higher breaking tendency of the composites [20-22].

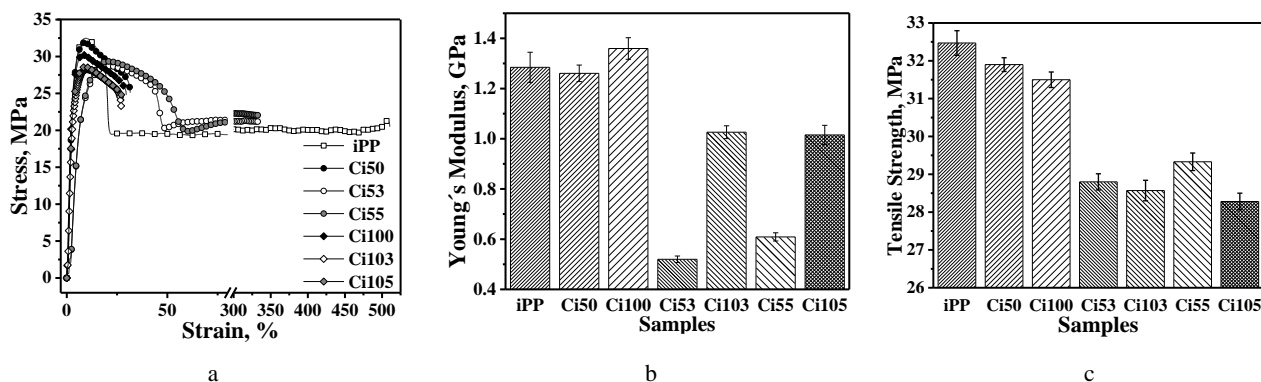


Fig. 3. Tensile test results of pure iPP and Ci50, Ci53, Ci55, Ci100, Ci103, and Ci105 composites: a–stress-strain curves of all samples; b–Young's modulus; c–tensile strength

Ci53 and Ci55 composites exhibit ductility above 300 % of strain, it's due to a similar proportion amount and characteristics mechanical of POE-g-MAH. In the case of Ci103 and Ci105 with POE-g-MA the ductility exhibited 30.72 and 35.22 %, respectively. Here, it had no increase in the ductility due amount exceed in 5 % of CW, and then it reduced of mobility of molecular chains [17]. Fig. 3 b shows Young's modulus of the pure iPP and composites. For reference, the pure iPP has an E of 1284 MPa. For Ci50 sample, there is a slight reduction of Young's modulus (1260 MPa) due to the addition of 5 % of the CW.

The decrease in Young's modulus suggests poor stress transfer from the polymer matrix to the inorganic particles [20, 25]. The composites with POE-g-MAH compatibilizer (Ci53 and Ci55) provided a decrease in Y of around 50 % (519.96 MPa and 609.94 MPa, respectively) which indicates a reduction in stiffness, due to the addition of the POE-g-MAH [21]. The Ci100 sample exhibited Young's modulus of 1359 MPa, which is an increase compared to the pure iPP sample. Then Young's modulus depends on a load of particles [22, 26]. Ci103 and Ci105 with POE-g-MAH were greatly affected in Young's modulus values (1026.12 and 1015.23 MPa, respectively). So that, the stiffness of such samples decreased, both; due to a similar proportion load of particles and compatibilizing agent percentage. During the tensile test was observed a debonding that produced at the interface between the matrix and compatibilizing agent, and not at the interface between POE-g-MAH and particle. Therefore, the mechanical properties of the iPP/CW composites depend mainly on the

interaction of the interface between iPP and compatibilizer [27]. According to Fig. 3 c, the tensile strength (σ_m) was determined for pure iPP and composites. Pure iPP had a σ_m of 32.47 MPa. The composites showed decreased tensile strength. There is a slight drop in Ci50 and Ci100 composite (31.9 and 31.3 MPa, respectively). It is observed that after the filler with the matrix and poor adhesion between the filler and the matrix [20]. The effect of the POE-g-MAH addition is more evident in a decrease of σ_m in composites. It is attributed to the fact that the fillers that do not contribute to the stress had been transferred to the polymeric matrix by an irregular shape. In this way, the incorporated material acts as a filler rather than a reinforcement. The behavior of the composites is associated with inadequate wetting of the incorporation of CW in the matrix iPP.

Fig. 4 shows the results of the flexural tests. Fig. 4 a presents the behavior of the flexure stress versus deflection curves during the test of pure iPP and composites at room temperature, which shows that there is no fracture in the specimens with deflection above 30 % with the addition of CW and POE-g-MAH. In Fig. 4 b, it is shown that the flexural modulus of pure iPP was 888.02 MPa. Ci50 and Ci100 without a compatibilizing agent showed an E_f of 907.58 and 905.77 MPa, respectively. So, there was an increase with respect to pure iPP, which is attributed to the amount of CW in the iPP matrix and the reduction in the mobility of the molecular chains [17]. Ci103 and Ci105 composites showed a slight decrease of 868.44 and 861.37 MPa, respectively, with respect to pure iPP.

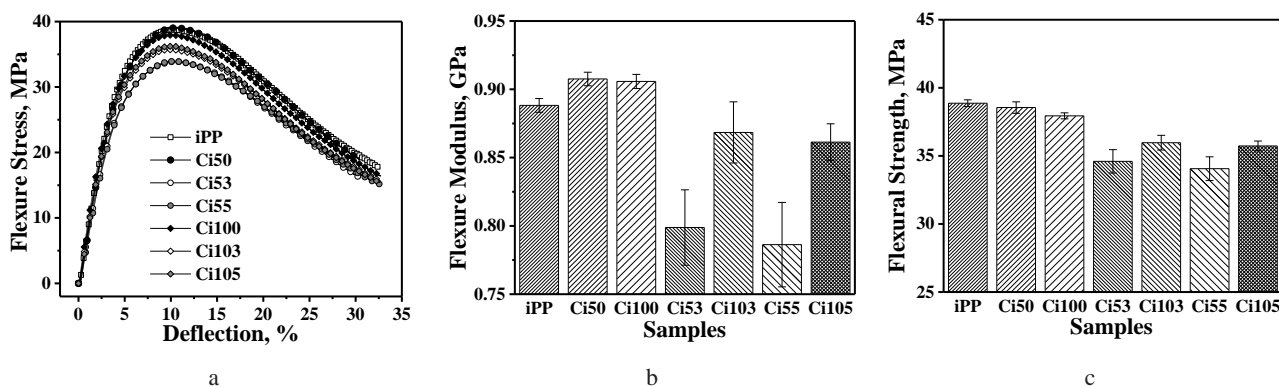


Fig. 4. Flexural test of pure iPP and Ci50, Ci53, Ci55, Ci100, Ci103, and Ci105 composites to room temperature: a–flexure stress-deflection; b–flexure modulus; c–flexural strength

Not so for the Ci53 and Ci55 composites (798.84 and 786.30 MPa, respectively) shown a decreased Flexural modulus. This phenomenon is due to low Flexure modulus and effect lubrication of the POE-g-MAH [16].

Fig. 4 c shows the flexural strength (σ_{fm}) measurements. The pure iPP obtained 38.57 MPa of σ_{fm} . For Ci50 and Ci100 composites, σ_{fm} was 38.85 and 37.94 MPa, respectively. There is a similar σ_{fm} . So, it is not considered a reduction in this mechanical property, in this case, acting as a filler. These values were obtained because they do not have a POE-g-MAH, and the CW reduces the molecular mobility of the chains. The CW had a better mechanical behavior on the matrix surface, achieving a better matrix/particle adhesion [17]. On the other hand, the resistance and stiffness reduction effect was observed for the composites Ci53, Ci55, Ci103, and Ci105 with POE-g-MAH, the values of 34.6, 34.0, 35.97, and 36.22 MPa, respectively. This phenomenon is due to POE-g-MAH by the lubrication or plasticizing effect, already mentioned above. Fig. 5 shows the measurements of Hardness Rockwell R (HRR). The value for pure iPP was 85.74 HRR. The composites Ci50 and Ci100 were 92 HRR, both. This indicates that the addition of CW into the iPP matrix increased the hardness due to the physical characteristics of particles and contributed to the hardness and stiffness of the CW/iPP composites. The incorporation of POE-g-MH (Ci53, Ci55, Ci103, and Ci105) in the iPP/CW was like their hardness to pure iPP (85, 84, 85, and 83 HRR) Then, the increment of hardness also is due to the increase of density, so that added amount of CW result in this physical change [28]. In this case, the addition of POE-g-MAH reduced slightly HRR due to the low hardness polymer and lubrication effect [16, 26].

3.3. Analysis of fracture surface of the mechanical testing

SEM microscopy was used to evaluate the fracture in the surface of the composites after the tensile test (Fig. 6). Cavities were observed throughout the matrix in all samples, particularly inside holes where some CW particles were found.

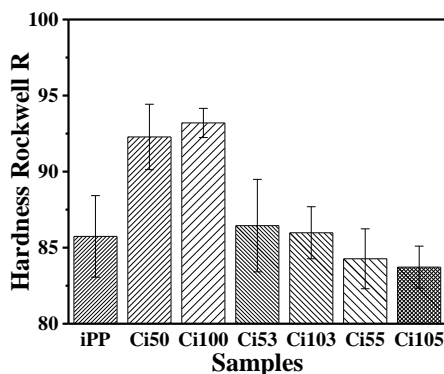


Fig. 5. Hardness test of pure iPP and composites

So, this indicates that there is not enough interfacial adhesion between the CW and iPP matrix. The type of interfacial interaction observed was by mechanical adhesion (Fig. 6 a and e), which represents a fit connection to the shape of the surface of the CW particle, which generates an effect at the macroscopic level. During the injection process, the molten low viscosity iPP filled pores of a minimum size

of 2 μm but not the entire surface of the CW particle, resulting in a weak mechanical adhesion between the two components once the iPP has hardened or solidified [29]. As a consequence that stress cannot be efficiently transferred from the matrix to the fillers. Fig. 6 b and f correspond to Ci50 and Ci100 to composites without a compatibilizing agent. The matrix fracture of the Ci50 and Ci100 composites seems to be omnidirectional. The fracture in Ci53, Ci55, Ci103, and Ci105 with POE-g-MAH were showed an orientation of the iPP matrix after fracture (Fig. 6 c, d, g, and h) exhibited similarities in the deformation direction of the matrix.

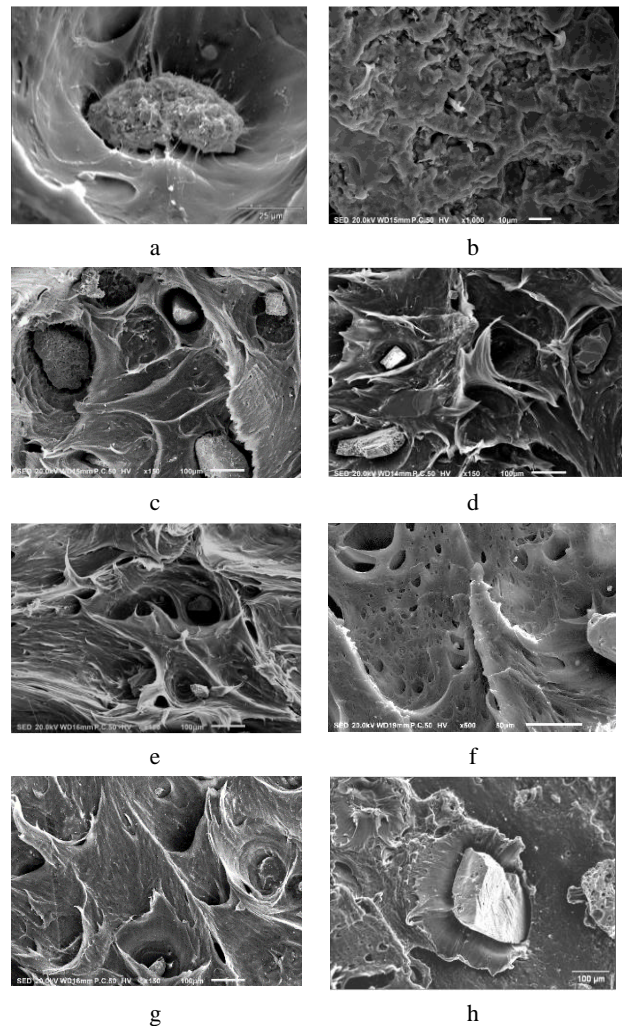


Fig. 6. SEM images fracture surface composites after tensile test: a, e—interfacial interaction by mechanical adhesion composites; b—Ci50; c—Ci53; d—Ci55; f—Ci100; g—Ci103; h—Ci105 composites

This irregularity could be attributed to demonstrating lower matrix strength under the stress produced by the addition of the POE-g-MAH [20]. As was observed in SEM images, POE-g-MAH did not enhance the interface interaction between CW and the iPP matrix. Therefore, the tensile and flexural strengths of the composite materials decreased. It can be confirmed that the roughness of the surfaces favors adhesion in most cases due to a high degree of surface activity caused by the creation of defects in the matrix, such as shrinkage, porosity, dimensional contractions, etc. But too much roughness in the CW particles can lead to a decrease in resistance, which can be

attributed to the development of localized stress peaks and the presence of cavities, and as a result, the reduction in the number of contact points [29].

Fig. 7 shows a comparison by SEM of the fracture surface obtained from the composites flexural test. Fig. 7 a and d shows the fracture surface of Ci50 and Ci100 composite after the test, in which a brittle fracture between iPP matrix and CW is observed. In this fracture, a relatively smooth fracture surface of the composite with the CW particles embedded in the matrix is observed. The CW particles adhering to the matrix indicate that there is a better mechanical adhesion due to the transferred stress, and it is shown in the increase in the flexural modulus. It is due to the compressive stresses of the matrix on the particles that hinder the displacement of the matrix or the propagation of the crack during the deformation of the sample and, therefore, during the fracture [21].

The Ci53, Ci55, Ci103, and Ci105 composites shown in Fig. 7 (b, c, e, and f), exhibit a weak adhesion interaction between the CW and iPP matrix since a detachment of the CW particles and a great deformation through the matrix. So, the flexural strength, flexural, and Young's modulus were affected because the stress cannot be efficiently transferred from the matrix to the CW particles due to the addition of POE-g-MAH and its effect [20].

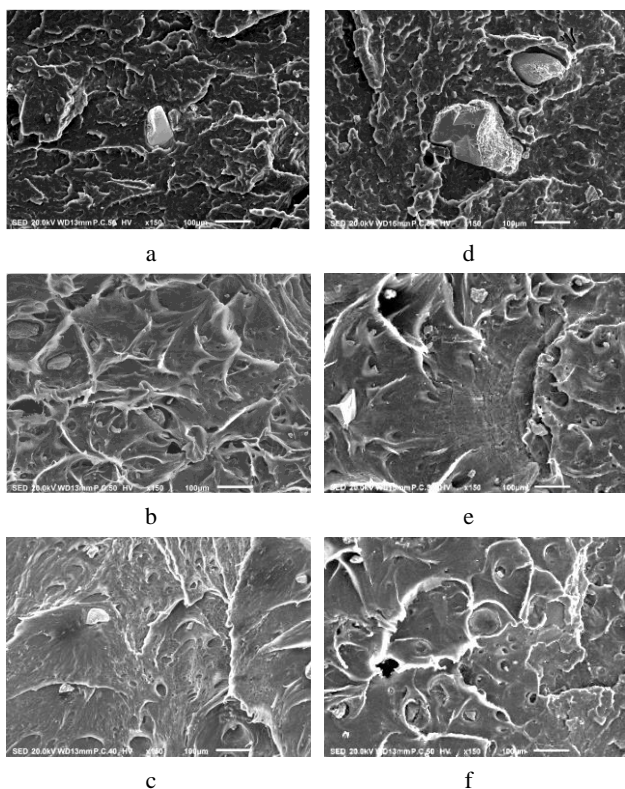


Fig. 7. SEM images cryogenic fractured composites after flexural test: a–Ci50; b–Ci53; c–Ci55; d–Ci100; e–Ci103; f–Ci105 composites

3.4. Crystalline structure of composites

XRD patterns of pure iPP and composites are shown in Fig. 8. XRD pattern of iPP exhibits seven peaks which correspond to the α -monoclinic phase of the isotactic polypropylene (JCPDS-00-050-2397). The XRD pattern of the sample exhibits six main peaks which correspond to the

mullite structure (JCPDS-01-079-1276), and five that correspond to the zirconium silicate (JCPDS-06-266), see Fig. 1 a.

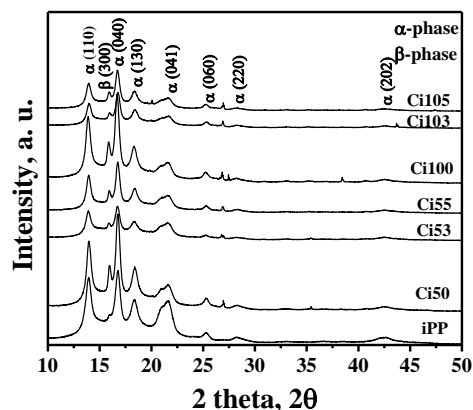


Fig. 8. XRD pattern of pure iPP and composites

All composites showed the characteristic peaks of the α -monoclinic phase planes (110), (040), (130), (041), (060), (220), and (202), and a small peak of the β -hexagonal phase (300). With the addition of CW in pure iPP, the β -hexagonal peaks appeared at $2\theta = 15.9^\circ$, which is observed in all composites [21, 27, 30]. In all composites, a reduction in peak intensity and sharpness were evident because of a lessening in the amount of the polymer matrix, as evidenced in Fig. 8. The addition of CW to the pure iPP generated an effect on the nucleation and growth of the α phase ($2\theta = 13.9^\circ$ (110), 16.7° (040), 18.4° (130)), and β phase ($2\theta = 15.9^\circ$ (300)) phases. According to the literature, the increase of the β phase in pure iPP is dependent on the content of CW or reinforcement [27]. However, when POE-g-MAH was added to compounds Ci53, Ci55, Ci103, and Ci105, the intensity of the X-ray diffraction peaks of the α and β phases decreased but did not change the diffraction angles [31].

Table 2 presents the crystallite size relationship, 2 theta and the planes of the α phase (110), (040), (130), and the β phase (300) for pure iPP and composites.

Table 2. XRD data of pure iPP and composites

Phase/hkl	2θ	Crystallite size, nm						
		iPP	Ci50	Ci53	Ci55	Ci100	Ci103	Ci105
α /(110)	13.92	10.1	13.5	9.2	13.3	17.9	13.9	13.2
β /(300)	15.94	0.00	13.3	9.4	10.5	12.8	7.0	12.0
α /(040)	16.78	11.1	15.3	10.9	15.3	16.7	15.7	15.5
α /(130)	18.40	6.7	7.9	5.7	7.1	10.1	8.8	9.1

The crystallite size was calculated by means of Scherrer's equation for the pure iPP characteristic intensity peaks planes: α -phase (110) = 10.1, α -phase (040) = 11.1, α -phase (130) = 6.74 nm. For Ci50 and Ci100 were (110) = 13.5 and 17.9 nm, (040) = 15.3 and 16.7 nm, (130) = 7.9 and 10.1 nm, and β phase (300) = 13.3 and 12.8 nm. Comparing the sizes with respect to pure iPP, there is an increase in crystallite size for composites. The growth of crystallite was observed as an increase in the preferential orientation of growth in the plane (110), (040), and (130) for all composites [32, 33]. A relationship was observed between crystallite size and Young's modulus of these composites. Due to crystallite size increases in the Ci50 and Ci100 composites; Young's modulus improved, but not so

for the Ci53, Ci55, Ci103, and Ci105 composites with the compatibilizer that show a similar crystallite size (Table 2), and due there is the lubrication effect of the POE-g-MAH; Young's modulus decayed. This denotes important behavior in stiffness, strength tensile, flexural modulus, flexural strength, and HRR mechanical properties.

The percentage of crystallinity (X_c , %) was determined using the EVA software by calculating the area under the curve of the main indexed peaks of phase α (110), (040), (130), (041), (060), and the β (300) phase of pure iPP and composites (Table 3). So, the percent crystallinity in pure iPP was 32.02 %, but when 5 and 10 wt.% CW were added, they were 87.88 % and 80.54 % for Ci50 and Ci100, respectively. Thus, the effect of the addition of the CW promoted an increase in X_c , % generating nucleation sites and orientation of the iPP molecule chains around the CW [32, 33]. Likewise, it was observed that the peaks of the α phase planes (110), (040), and (130) are finer due to the increase in the degree of crystallinity and the preferential orientation in these mentioned planes. The increase in X_c , % and the appearance of the β -phase induced by CW processing led to a further improvement of the flexural and Young's modulus, and the flexural strength of the Ci50 and Ci100 composites. On the other hand, the addition of POE-g-MAH caused a decrease in the degree of crystallinity; the values were 58.37 %, 58.15 %, 68.64 %, and 69.68 % for Ci53, Ci55, Ci103, and Ci105, respectively [30]. Thus, it shows that the immiscibility of the POE-g-MAH with the iPP matrix and the decrease in the degree of crystallinity due to the lack of interfacial interaction between the CW particles and the iPP implies the mechanical properties obtained, which are reduced by adding POE-g-MAH [34].

FTIR spectra shown in Fig. 9 present the characteristic bands of pure iPP, CW, POE-g-MAH, and composites.

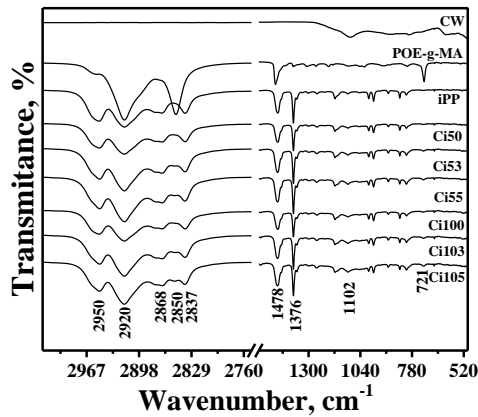


Fig. 9. FTIR spectra of pure iPP and composites

Table 3. DSC, XRD and TGA data of iPP pure and composites

Composite	T_c , °C	T_c onset, °C	ΔH_c , J/g	T_m - β , °C	T_m - α , °C	ΔH_m , J/g	T_{deg} , °C TGA	X_c , % DSC	X_c , % XRD
iPP	110.48	115.56	135.41	0	165.67	61.87	376.4	29.60	32.08
Ci50	117.35	121.11	225.06	162.21	168.02	191.93	404.8	89.83	87.88
Ci53	115.32	119.46	155.17	160.57	165.23	127.05	403.5	60.78	58.37
Ci55	114.68	118.99	170.72	161.57	166.37	144.56	401.3	69.16	58.15
Ci100	117.38	124.87	141.17	161.40	167.02	182.19	403.1	87.17	80.54
Ci103	115.94	120.07	129.79	161.59	164.92	103.12	407.0	49.33	68.64
Ci105	115.43	119.83	138.19	161.59	166.59	139.43	410.6	66.71	69.98

IR spectrum of the pure iPP shows the characteristic vibration stretching bands of CH located between 2800–3000 cm^{-1} , and the bending vibration bands of CH_2 are at 1478 cm^{-1} and 1376 cm^{-1} . IR spectrum of the POE-g-MAH presents two stretching vibration bands due to CH at 2850 and 2920 cm^{-1} . The weak rocking CH_2 vibration band is located at 721 cm^{-1} . In the composites with POE-g-MAH compatibilizer, there is partial miscibility between compatibilizer and iPP, and a low transmittance band is observed at 721 cm^{-1} due to amounts of POE-g-MAH agent compatibilizer. But the addition of POE-g-MAH increases transmittance in the composites in the bands of iPP [35]. FTIR spectrum of the CW show the band attributed to the stretching vibration of the Si-O-Si bond at 1102 cm^{-1} . The addition of CW in the matrix reduces transmittance in the range of 1300 to 2980 cm^{-1} . The FTIR showed that the chemical structures of the composites were similar and that there were no major changes among the composites, this confirms the type of interfacial interaction mechanism by mechanical adhesion [28].

3.5. Thermal behavior of composites

Table 3 and Fig. 10 show the thermal analysis obtained by DSC of pure iPP and its composites. The thermal properties such as crystallization temperature (T_c), crystallization temperature onset (T_c onset), crystallization enthalpy (ΔH_c), α and β melting temperature (T_m), melting enthalpy (ΔH_m), the degree of crystallinity DSC and XRD (X_c , %) is summarized in Table 3. The crystallinity percentage (X_c , %) was determined from the melting enthalpy values using the following Eq. 2 [27]:

$$X_c\% = \frac{H_m}{(1-\alpha)H_m} \times 100, \quad (2)$$

where H_m is the melting enthalpy of the specimens, J/g; H_m is the enthalpy value for a theoretically 100% crystalline PP (209 J/g); $(1 - \alpha)$ is the weight fraction of polymer in the pure iPP and composites. DSC results show the effect of CW and POE-g-MAH on the crystallization behavior in iPP, which is demonstrated by non-isothermal crystallization. The non-isothermal crystallization curves of iPP and composites running at a cooling rate of 10 °C/min are shown in Fig. 10 a. The crystallization peak temperature of pure iPP is located at 110.48 °C. As seen from table 3, either CW (5 and 10 wt.%) and POE-g-MAH (3 and 5 wt.%) to pure iPP led to a slight increase in the values of T_c onset, and T_c for iPP crystallization. However, the effect on T_c onset and T_c caused by CW was a bit higher (about 117 °C) than that by POE-g-MAH (about 115 °C), which implies that CW played a preferable nucleation agent role in iPP crystallization.

With the content of POE-g-MAH from 3 to 5 wt.% were a slight decrease of T_c onset, and T_c (below 120.0 °C) indicates the weakened nucleation effect of CW on iPP crystallization in blends, which corresponded to the CW distribution in these blends. This could be explained by the weakened interaction between CW particles and iPP molecules attributable to the incorporation of POE-g-MAH [12]. The melting temperature (T_m) (Table 3) of the iPP in the α -phase was 165.67 °C. When the CW was incorporated into the iPP matrix, the curves exhibit a double endothermic peak: the α -phase and β -phase (Fig. 10 b). The α -phase melting temperature, in the case, of Ci50 and Ci100 were 168.02 and 167.02 °C, respectively. In a similar way, another endothermic peak induced by CW is the formation of the β -phase. The T_m of the β -phase was about 161.48 °C at all curves.

It is evident that CW was added to increase the T_m in the composites. The change in melting point in iPP can be attributed to the reduction of the chain flexibility [28, 37, 38]. An increase of T_m introduces higher undercooling of the melt and higher size of spherulites [26, 39]. POE-g-MAH was added, and the T_m was slightly reduced, it was not a significant effect. The heat of melting enthalpy (ΔH_m) showed that pure iPP was 61.87 J/g. Compare ΔH_m with Ci50 and Ci100 composites were higher (up 180 J/g) than iPP, indicating a dilution effect owing to the substitution of some iPP by CW [40]. When added POE-g-MAH, the ΔH_m was below 140 J/g. The area of the melting peak assigned to the α -phase was larger than that of the β -phase, suggesting a higher content of the α -phase [41].

The X_c , % by DSC analysis for the iPP matrix was 29.6 %. But the addition of CW and POE-g-MAH modified it. The composites Ci50 and Ci100 increased the X_c , % to 89.83 and 87.17 %, respectively, and indicate that the CW worked as agent nucleation, increasing the nucleation points in the matrix. So, CW retained heat and promotes the establishment and crystallization of molecular chains. The results suggested that CW could not only work as an effective β -nucleating agent for iPP but also accelerate the arrangement of macromolecule chains to form a regular structure [36]. This behavior is related to the increase of Young's modulus in the composites Ci50 and Ci100, improving the stiffness. However, when POE-g-MAH compatilizing agent has been added, an important change is observed in the X_c ,%. X_c , % of the Ci53, Ci55, Ci103, and Ci105 were below 69%. This is a consequence of the interface's low compatibility between the iPP and the

polyolefin elastomer main chain of the POE-g-MAH. The inhibition effect on the crystallization of composites may lead to the decrease of tensile and flexural strengths, which coincided with the results of mechanical properties [20].

Fig. 10 c and Table 3 show the thermal degradation analysis behavior (TGA) of pure iPP and composites under an inert argon atmosphere. The onset temperature (T_{deg}) corresponds to 5 % mass loss. The pure iPP exhibits a 5 % mass loss at 376.4 °C. In comparison, Ci105 exhibited a 410 °C increase in its T_{deg} relative to pure iPP. A minimum and maximum increase in T_{deg} 28.4 °C and 33.6 °C is observed in composites containing 5 and 10 wt.% CW, respectively. The presence of well-dispersed CW in the iPP matrix is expected to provide a barrier to the diffusion of degradation products, suppressing iPP mass loss in the composite [42].

4. CONCLUSIONS

Composites based on an iPP matrix with ceramic waste and an incorporated POE-g-MAH compatilizing agent were prepared by means of an extrusion and injection molding process. The compounds showed homogeneity and good dispersion, and without the presence of agglomerates of CW particles in the iPP matrix, and thus also with the incorporation of POE-g-MAH. During the mechanical test, it was determined that the CW particles added to the pure iPP decreased the ductility by reducing the mobility of the molecular chains and produced an increase in the stiffness and hardness of the composites without POE-g-MAH. Flexural strength was not significantly affected in Ci50 and Ci100 composites of 5 and 10 % CW. Consequently, CW increased the degree of crystallinity and the size of the crystallites of the α phase, and the nucleation and growth of the β phase. Therefore, the effect on the flexural modulus and Young's modulus was observed, which strongly depended on the CW particle loading. So, with these properties, the composite material can be applied in low-load structural components or as a filler to reduce the virgin polymer, see Fig. 11 (component injected with Ci50 composite).

So, the CW acted as a filler and nucleating agent. On the other hand, the addition of POE-g-MAH affected the mechanical properties very clearly. The debonding behavior takes place at the interfaces between the iPP/POE-g-MAH/CW particles. Regarding the thermal behavior, it was better when CW was added, achieving an increase in the melting temperature of all the compounds.

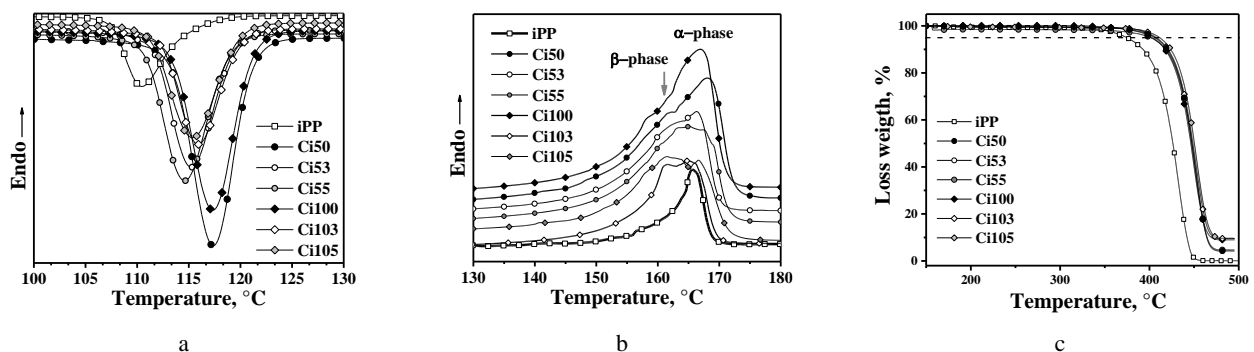


Fig. 10. DSC analysis: a–crystallization; b–melting curves; c–TGA analysis for pure iPP and composites



Fig. 11. Simple product injection with Ci50 composite

The addition of CW and POE-g-MAH to the iPP matrix achieved an increase in the melting temperature and the crystallinity temperature, which favored the thermal stability that is observed in the increase in the degradation temperature. In general, the addition of CW produced interesting results, which could generate a line of research by modifying the particle size and the type of compatibilizing agent. Then, the issue of reusing residual ceramics shows a favorable trend to promote sustainability.

Acknowledgments

Financial support for this work was provided by PRODEP, Project Number: ITESJOCO-PTC-13. CAE Department-TEJJo. Manufacturing company supply raw materials.

REFERENCES

- Kumar-Sharma, A., Baredar, P.** Development of the Composites by Using Industrial Waste *Materials Today Proceedings* 18 (7) 2019: pp. 5128–5132. <https://doi.org/10.1016/j.matpr.2019.07.509>
- Mark, U.C., Mark, U.** Improving the Mechanical Properties of Polypropylene Composites with Coconut Shell Particles *Composites and Advanced Materials* 30 2021: pp. 1–9. <https://doi.org/10.1177/26349833211007497>
- Girge, A., Goel, V., Gupta, G., Fuloria, D., Ranjan-Pati, P., Sharma, A., Kumar-Mishra, V.** Industrial Waste Filled Polymer Composites – A Review *Materials Today: Proceedings* 47 (11) 202: pp. 2852–2863. <https://doi.org/10.1016/j.matpr.2021.03.617>
- Singh, R., Singh, I., Kumar, R., Brar, G.S.** Waste Thermosetting Polymer and Ceramic as Reinforcement in Thermoplastic Matrix for Sustainability: Thermomechanical Investigations *Journal of Thermoplastic Composites Materials* 34 (4) 2021: pp. 523–535. <https://doi.org/10.1177/0892705719847237>
- Hanagiri, S., Shimpo, A., Inuzuka, T., Sakaki, S., Matsui, T., Aso, S., Matsuda, T., Nakagawa, H.** Recent Improvement of Recycling Technology for Refractories *Nippon Steel Technical Report* 98 2008: pp. 93–98.
- Velasco-Parra, J.A., Ramón-Valencia, B.A., Mora-Espinosa, W.J.** Composite Materials Reinforced with Ceramic Waste and Matrix of Unsaturated Polyester for Applications in the Automotive Industry *DYNA* 87 (212) 2020: pp. 251–258. <http://doi.org/10.15446/dyna.v87n212.81483>
- Anggono, J.** Mullite Ceramics: Its Properties, Structure, and Synthesis *Jurnal Teknik Mesin* 7 (2) 2005: pp. 1–10.
- Švab, I., Musil, V., Leskov, M.** The Adhesion Phenomena in Polypropylene/Wollastonite Composites *Acta Chemical Slovenica* 52 2005: pp. 264–271.
- Zhu, S., Chen, J., Zuo, Y., Li, H., Cao, Y.** Montmorillonite/Polypropylene Nanocomposites: Mechanical Properties, Crystallization and Rheological Behaviors *Applied Clay Science* 52 2011: pp. 171–178. <http://doi.org/10.1016/j.clay.2011.02.021>
- Juhasza, J.A., Besta, S.M., Brooks, R., Kawashita, M., Miyata, N., Kokuboc, T., Nakamura, T., Bonfield, W.** Mechanical Properties of Glass-Ceramic A–W–Polyethylene Composites: Effect of Filler Content and Particle Size *Biomaterials* 25 2004: pp. 949–955. <http://doi.org/10.1016/j.biomaterials.2003.07.005>
- Maris, J., Bourdon, S., Brossard, J.M., Cauret, L., Fontaine, L., Montembault, V.** Mechanical Recycling: Compatibilization of Mixed Thermoplastic Wastes *Polymer Degradation and Stability* 147 2018: pp. 245–266. <https://doi.org/10.1016/j.polymdegradstab.2017.11.001>
- Liang, J.Z.** Impact Fracture Toughness and Flow Properties of Polypropylene Composites *Polymer Testing* 60 2017: pp. 381–387. <http://dx.doi.org/10.1016/j.polymertesting.2017.04.022>
- Zhong, W., Qiao, X., Sun, K., Zhang, G., Chen, X.** Polypropylene–Clay Blends Compatibilized with MAH-g-POE *Journal of Applied Polymer Science* 99 2005: pp. 2558–2564. <https://doi.org/10.1002/app.22880>
- Shen, H., Wang, Y., Mai, K.** Effect of Compatibilizers on Thermal Stability and Mechanical Properties of Magnesium Hydroxide Filled Polypropylene Composites *Thermochimica Acta* 483 2009: pp. 36–40. <https://doi.org/10.1016/j.tca.2008.10.025>
- Wahit, M.U., Hassan, A., Mohd Ishak, Z.A., Czigan, T.** Ethylene-Octene Copolymer (POE) Toughened Polyamide 6/Polypropylene Nanocomposites: Effect of POE Maleation *Express Polymer Letters* 3 2009: pp. 309–319. <https://doi.org/10.3144/expresspolymlett.2009.39>
- Ji-Zhao, L., Bo, Z., Wen-Yong, Ma.** Morphology and Mechanical Properties of PP/POE/Nano-CaCO₃ Composites *Polymer Composites* 37 (2) 2014: pp. 539–546. <https://doi.org/10.1002/pc.23210>
- Qiao, X., Zhong, W., Sun, K., Chen, X.** Effects of Clay Contents on the Dynamic Mechanical and Rheological Properties of Polypropylene/MAH-g-POE/Clay Composites *Journal of Applied Polymer Science* 114 2009: pp. 1702–1709. <https://doi.org/10.1002/app.30218>
- Lin, Z., Chen, C., Guan, Z., Tan, S., Zhang, X.** A Compatibilized Composite of Recycled Polypropylene Filled with Cellulosic Fiber from Recycled Corrugated Paper Board: Mechanical Properties, Morphology, and Thermal Behaviour *Journal of Applied Polymer Science* 122 2011: pp. 2789–2797. <https://doi.org/10.1002/app.34321>
- Bishnoi, A., Kumar, S., Joshi, N.** Chapter 9. Microscopy Methods in Nanomaterials Characterization Micro and Nano Technologies: Wide-Angle X-ray Diffraction (WAXRD): Technique for Characterization of Nanomaterials and Polymer Nanocomposites *Elsevier* 2019: pp. 313–337. <https://doi.org/10.1016/B978-0-323-46141-2.00009-2>
- Kaya, N., Atagur, M., Akyuz, O., Seki, Y., Sarikanat, M., Sutcu, M., Seydibeyoglu, M.O., Sever, K.** Fabrication and

- Characterization of Olive Pomace Filled PP Composites *Composites Part B* 150 2018: pp. 277–283.
<http://dx.doi.org/10.1016/j.compositesb.2017.08.017>
21. Wang, X., Song, R., Guo, K., Chen, Y., Zhao, Y., Zhu, K., Yuan, X. High Impact Strength for Polypropylene/Titanate Whisker Composites with Dual Compatibilizing *Polymer Composites* 40 (9) 2019: pp. 3420–3428.
<https://doi.org/10.1002/pc.25203>
 22. Dang, L., Nai, X., Zhu, D., Xu, N., Dong, Y., Li, W. Effects of Different Compatilizers on Mechanical, Crystallization and Thermal Properties of Polypropylene/Magnesium Oxysulfate Whisker Composites *Journal of Adhesion Science and Technology* 31 (16) 2017: pp. 1839–1857.
<https://doi.org/10.1080/01694243.2017.1285386>
 23. Yaoa, Z.T., Chenb, T., Lic, H.Y., Xiab, M.S., Yeb, Y., Zheng, H. Mechanical, and Thermal Properties of Polypropylene (PP) Composites Filled with Modified Shell Waste *Journal of Hazardous Materials* 262 2013: pp. 212–217.
<http://dx.doi.org/10.1016/j.jhazmat.2013.08.062>
 24. Zhai, W., Wang, Y., Deng, Y., Gao, H., Lin, Z., Li, M. Recycling of Asbestos Tailings Used as Reinforcing Fillers in Polypropylene-Based Composites *Journal of Hazardous Materials* 270 2014: pp. 137–143.
<http://dx.doi.org/10.1016/j.jhazmat.2014.01.052>
 25. El-Midany, A.A., Ibrahim, S.S. The Effect of Mineral Surface Nature on the Mechanical Properties of Mineral-Filled Polypropylene Composites *Polymer Bulletin* 64 2010: pp. 387–399.
<http://dx.doi.org/10.1007/s00289-009-0209-x>
 26. Khan, Z.I., Habib, U., Binti Mohamad, Z., Bin Rahmat, A.R., Binti Abdullah, N.A.S. Mechanical and Thermal Properties of Sepiolite Strengthened Thermoplastic Polymer Nanocomposites: A Comprehensive Review *Alexandria Engineering Journal* 61 2021: pp. 1–16.
<https://doi.org/10.1016/j.aej.2021.06.015>
 27. Wang, Y., Shen, H., Li, G., Mai, K. Effect of Interfacial Interaction on the Crystallization and Mechanical Properties of PP/Nano-CaCO₃ Composites Modified by Compatibilizers *Journal of Applied Polymer Science* 113 2009: pp. 1584–1592.
<https://doi.org/10.1002/app.30057>
 28. Deniz, A., Gulsen, U., Havva, G., Sonnur, Y., Sultan, G., Timucin, B., Gokhan, G. Nanocomposites of Polypropylene/Nano Titanium Dioxide: Effect of Loading Rates of Nano Titanium Dioxide *Materials Science (Medžiagotyra)* 22 (3) 2016: pp. 364–369.
<http://dx.doi.org/10.5755/j01.ms.22.3.8217>
 29. Tatjana, G., Stefan, J. Specialized Injection Moulding Techniques, Elsevier, USA, 2016: pp. 165–180.
 30. Kim, D.Y., Kim, G.H., Dong, Y.L., Seo, K.H. Effects of Compatibility on Foaming Behavior of Polypropylene/Polyolefin Elastomer Blends Prepared Using a Chemical Blowing Agent *Journal Applied Polymer Science* 134 2017: pp. 1–10.
<http://dx.doi.org/10.1002/APP.45201>
 31. Alanalp, M.B., Durmus, A. Quantifying Microstructural, Thermal, Mechanical, and Solid-State Viscoelastic Properties of Polyolefin Blend Type Thermoplastic Elastomer Compounds *Polymer* 142 2018: pp. 267–276.
<https://doi.org/10.1016/j.polymer.2018.03.054>
 32. Jain, K., Madhu, G., Bhunia, H., Bajpai, P.K., Nando, G.B., Reddy, M.S. Physico-Mechanical Characterization, and Biodegradability Behavior of Polypropylene/ Poly(L-lactide) Polymer Blends *Journal of Polymer Engineering* 35 (5) 2015: pp. 407–415.
<https://doi.org/10.1515/polyeng-2014-0179>
 33. Zhang, Z., Tao, Y., Yang, Z., Mai, K. Preparation, and Characteristics of Nano-CaCO₃ Supported β -nucleating Agent of Polypropylene *European Polymer Journal* 44 2008: pp. 1955–1961.
<https://doi.org/10.1016/j.eurpolymj.2008.04.022>
 34. Sengupta, S., Ray, D., Mukhopadhyay, A. Polypropylene and Fly Ash Using a Green Coupling Agent *ACS Sustainable Chemistry & Engineering* 1 2013: pp. 574–584.
<https://doi.org/10.1021/sc3000948>
 35. Zhu, B., Zhang, J., Wang, J., Liu, J., Zhang, J. Compatibilisation of Multi-Monomer Grafted Poly(ethylene-co-octene) on Polypropylene/ Organo-Montmorillonite Nanocomposite *Plastics, Rubber and Composites* 47 (2) 2018: pp. 65–71.
<https://doi.org/10.1080/14658011.2017.1411866>
 36. Nan-Ying, N., Qin-Jian, Y., Feng, L., Qin, Z., Rongni, D., Qiang, F. Crystallization Behavior and Mechanical Properties of Polypropylene/Halloysite Composites *Polymer* 48 2007: pp. 7374–7384.
<https://doi.org/10.1016/j.polymer.2007.10.005>
 37. Buasri, A., Chaiyut, N., Borvornchettanuwat, K., Chantanachai, N., Thonglor, K. Thermal and Mechanical Properties of Modified CaCO₃/PP Nanocomposites *International Scholarly and Scientific Research & Innovation* 6 (8) 2012: pp. 689–692.
 38. Sahebian, S., Zebarjad, S.M., Vahdati Khaki, J., Sajjadi, S.A. The effect of Nano-Sized Calcium Carbonate on Thermodynamic Parameters of HDPE *Journal of Materials Processing Technology* 209 2009: pp. 1310–1317.
<http://dx.doi.org/10.1016/j.jmatprotec.2008.03.066>
 39. Polt, G., Spieckermann, F., Wilhelm, H., Fischer, Ch., Schaffler, E., Bernstorff, S., Zehetbauer, M. Crystalline Plasticity in Isotactic Polypropylene Below and Above the Glass Transition Temperature *Express Polymer Letters* 9 (10) 2015: pp. 894–900.
<http://dx.doi.org/10.3144/expresspolymlett.2015.81>
 40. Hsien-Tang, C., Yao-Kuei, H. Compatibilization of Poly (Ethylene Terephthalate)/Polypropylene Blends with Maleic Anhydride Grafted Polyethylene-Octene Elastomer *Journal of Polymer Research* 13 2006: pp. 153–160.
<http://dx.doi.org/10.1007/s10965-005-9020-z>
 41. Wei, X., Mingwei, Y., Shaohong, S., Hao, S., Min, N. Simultaneous Durability, and Strength Enhancement of β -Polypropylene Through Montmorillonite and Melt-Soluble β -Nucleating Agent Addition *Polymer Testing* 65 2018: pp. 150–155.
<https://doi.org/10.1016/j.polymertesting.2017.11.024>
 42. Iyer, K.A., Torkelson, J.M. Green Composites of Polypropylene and Eggshell: Effective Biofiller Size Reduction and Dispersion by Single-Step Processing with Solid-State Shear Pulverization *Composites Science and Technology* 102 2014: pp. 152–160.
<https://doi.org/10.1016/j.compscitech.2014.07.029>

